Simulation of the time resolution of a 50 μm low-gain avalanche detector.

C. Peña[*,a,b], G. Deptuch[a], S. Xie[b], A. Apresyan[a], L. Narvaez[b], T. Liu[a], N. Cartiglia[c]

[a] *Fermi National Accelerator Laboratory, Batavia, IL, USA*
[b] *California Institute of Technology, Pasadena, CA, USA*
[c] *INFN, Torino, Italy*

Abstract

In this paper we report simulation results on the timing resolution of a 50 μm low-gain avalanche detector (LGAD). The simulation includes: sensor fluctuations, front-end electronics, and quantization. Comparisons on the performance for different front-end electonics (FEE) bandwidths (BWs) are presented, as well as the dependance on singal-to-noise ratio (SNR). Two approaches to measure the timestamp are presented: leading edge (LE) and constant-fraction-discrimination (CFD). Aditionally, the time resolution is studied as function of the irradiation of the sensor. Simulated LGAD pulses before irradiation, and after neutron fluences of 5×10^{14} n/cm^2 and 1×10^{15} n/cm^2, are studied. The time resolution a 50 μm LGADs was found to be 30 ps for FE electronics BWs larger than 350 MHz and SNRs larger than 30. The time resolution at a SNR of 30 for fluences of 5×10^{14} n/cm^2 and 1×10^{15} n/cm^2 were found to be 30 ps and 40 ps, respectively.

Key words:
Silicon, Timing, LGAD

Contents

[*] Corresponding author
Email address: cmorgoth@fnal.gov (C. Peña)

1. Introduction

Future colliders, including the high luminosity upgrade of the Large Hadron Collider (HL-LHC) at CERN, will operate with an order of magnitude higher instantaneous luminosity compared to what has been achieved at the large hadron collider (LHC) so far. With the increased instantaneous luminosity, the rate of simultaneous interactions per bunch crossing (pileup) is projected to reach an average of 140 to 200. Pileup increases the difficulties in separating particles from the hard scattering interaction with those produced in different pileup interactions. In particular, the ability to discriminate between jets produced in the events of interests, especially those associated with vector boson fusion processes, and jets produced by pileup interactions will be degraded. Additionally, the efficiency to identify high p_{T} isolated electrons and muons will be severely reduced due to the high density of pileup particles in their vicinity. The missing transverse energy resolution will also deteriorate, and several other physics objects performance metrics will suffer the detrimental effects of pileup.

One way to mitigate the pileup effects mentioned above, complementary to precision tracking methods, is to perform a time of arrival measurement associated with each particle. Such a measurement with a precision of about 30-40 ps, will reduce the effective amount of pileup by a factor of 10, given that the spread in collision time of the pileup interactions at HL-LHC is foreseen to be approximately 200 ps. It has been previously shown that a precision of better than 20 ps can be achieved for electromagnetic showers measured with silicon sampling calorimeters [1–3] using traditional planar silicon detectors while precision of 30 ps can be achived for minimum ionizing particles (MIPs) measured with low-gain avalanches detectors (LGADs) [4–6].

LGADs are envisioned to be used in the CMS and ATLAS experiment upgrades for HL-LHC in order to overcome the event reconstruction challenges posed by the high rate of concurrent collisions per beam crossing. The implemented regions of pseudorapidity (η) are: $|\eta| > 1.5$, and $2.4 < |\eta| < 4.2$ for CMS and ATLAS, respectively. In order to achieve the desired timing precision across a large area of the detectors, the sensors will need to provide high uniformity of signal response and timing resolution. Beam test measurements have provided encouraging results towards achieving such detectors [4].

In this paper, we report simulation results on the timing resolution of a 50 μm low-gain avalanche detector (LGAD) which includes the effects of the sensor fluctuations, front-end electronics (FEE), and quantization. Our results indicate that for FEE analog bandwidths (BWs) larger than 350 MHz and signal-to-noise ratios (SNRs) larger than 30, measured at the output of the FFE, time resolutions of 30 ps and 40 ps are obtained when using time-walk corrections based on time-over-therhold (ToT) measurements to both timestamping techniques: constand-fraction-dricrimination (CFD) and leading-edge (LE), respectively. These results are compatible with previous measurements on LGAD timing resolutions carried out in laboratory and beam test conditions [4–6]. We study

the time resolution for four different FEE shaping times: 0.5 ps, 1.0 ps, 2.0 ps, and 4.0 ps; three SNR: 20, 30, 100; and three irradiation levels: pre-radiation, 5×10^{14} n/cm^2, and 1×10^{15} n/cm^2. For every point in this scan we evaluate the time resolution for LE and CFD.

The paper is organized as follows: the simulation is described in Sec. 2; algorithms used in the timing reconstruction and analysis are described in Sec. 3; simulation results are presented in Sec. 4, followed by the conclusion in Sec. 5.

2. Simulation Framework

The simulation framework is based on c++ programing language. The LGAD pulses are obtained from Weightfield2 (WF2), a 2-dimensional silicon simulator [**?**]. WF2 provides sets of 1000 LGAD pulses which models the response of the sensor to minimum ionizing particles (MIPs). We generated 3 sets of LGAD pulses for a 50 μm LGAD: pre-irradiation, and after neutron fluences of 5×10^{14} n/cm^2 and 1×10^{15} n/cm^2. The simulation framework takes the LGAD pulses (from WF2) and adds gaussian white noise (hereafter white noise). At this point the LGAD pulses with the added white noise are fed into the simulation of the FEE (see Fig. 1). The output of the FEE simulation is the convolution of the impulse response function and the input signal at the FEE. We consider four shaping constants for the impulse response of the FEE: 0.5, 1.0, 2.0, and 4.0 ns (the FEE simulation will be described in detail in Sec. 2.2). At the output of the FEE block we have a "realistic" LGAD pulse which includes the effects of sensor fluctuations, shaping of the FEE, and noise. A waveform analysis is performed with the pulses obtained at the output of the FEE block. We assign timestamps to each pulse by using algorithms that emulate an ideal LE discriminator and an ideal CFD. For each threhold we obtain a LE and CFD timestamps as well as the corresponding time-over-theshold (ToT) of the pulse. The SNR is defined as the ratio of the most probable value (MPV) of the amplitude distribution to the width of the amplitude distribution at a fixed sample (where only noise is present). We study 3 SNR scenarios: 20, 30, and 100. A schematic diagram of the simulation is shown in Fig. 1.

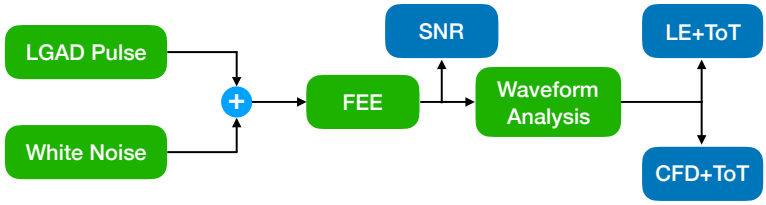

Figure 1: A schematic diagram of the simulation. Each simulation configurable block is shown in green. The most relevant outputs of the simulation are shown in blue.

2.1. LGAD pulse library and simulation

We need to ask Nicolo to send us a paragrah for the Weightfield2 (WF2)

2.2. Fron-end Electronics simulation and noise injection

The front-end simulation is implemented in c++ programing language. It combines analytical calculations when possible but it mostly relies on numerical methods. We implement most calculations in the time domain, while the frequency domain is mostly used to cross-check noise and the FEE expected response. Sections 2.2.1 and 2.2.2 detail the front-end and noise implementation in the simulation.

2.2.1. front-end implementation

The fron-end simulation is based on a single amplification stage. We focus on the BW of such amplifier rather than variations thereof. The fron-end chose is a second order low-pass filter which transfer function and impulse response are given by equations 1 and 2, respectively.

$$H(S) = \frac{\frac{1}{\tau_s^2}}{(S + 1/\tau_s)^2} \qquad (1) \qquad\qquad h(t) = \frac{t}{\tau_s^2} e^{-t/\tau_s} \qquad (2)$$

The output pulse of the FEE is the convolution (in time domain) of the pulse from the LGAD library and the FEE impulse response (see Eq. 2). The time base for the pulses and the convolution is 10 ps – this sampling time is used throughout the simulation. As stated above we focus the study on the BW of the FEE, to that end we scan the τ_s paremeter in Eq. 2 in the following set:{0.5, 1, 2, 4} ns, this parameter is hereafter referred to as shaping time (ST). Figure 2 (left) shows the comparison of the impulse and LGAD responses for a ST of 1 ns while Figure 2 (right) shows the LGAD response for all STs studied. We obseve that the LGAD response is delayed with respect to the impulse response, and that pulse slew rate is decreased in the first nanosecond of the pulse. We also observe the expected behavior when comparing the LGAD responses for the different STs, pulse risetimes scale with the ST and the decay time is dominated by the ST.

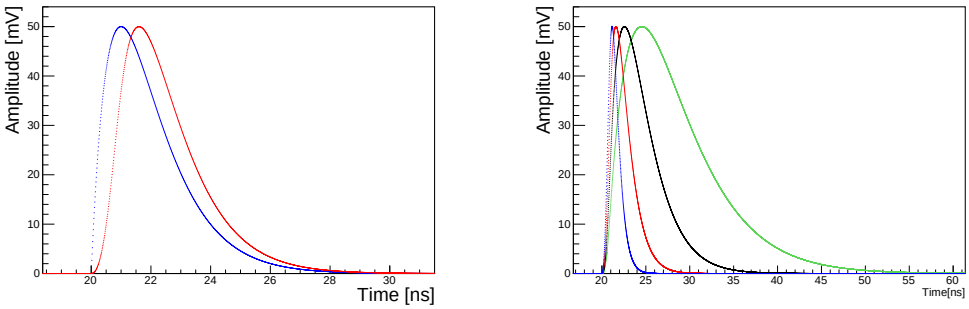

Figure 2: (Left) Comparison of impulse and LGAD reponses for the a shaping time (ST) of 1 ns. (Right) LGAD response for the four shaping times studied: {0.5, 1, 2, 4} ns. All pulses have been nomalized to achive a peak amplitude of 50 mV. Legends for the shaping times are shown in the plots.

Shaping time (ns)	0.5	1.0	2.0	4.0
Risetime (ns)	$0.7 \pm xx$	$0.9 \pm xx$	$1.4 \pm xx$	$2.5 \pm xx$

Table 1: Measured risetime for all shaping times studied: {0.5, 1, 2, 4} ns. Risetime is the $10\% - 90\%$ time difference as measured by the CFD algorithm described in Sec. 3.1.

2.2.2. noise injection

Gaussian white noise is simulated by sampling the full time window (0 - 100 ns) in 10 ps intervals. At each sampled time we assign a random amplitude which is drawn from from a gaussian distribution with zero mean and width corresponding to the SNR under study. It is important to note that the width of the gausian parameter is not exactly the SNR and needs to be adjusted depending on the ST of the FEE. The left panel of Figure 3 shows the gaussian white noise before and after a 1 ns FEE. The expected behavior for the noise is obtained. The left panel of Figure 3 shows the output of the FEE block, with a 1 ns ST, for a pre-radiation LGAD pulse when noise has been injected. The injected noise is such that the SNR is 30. SNR is defined ratio of the landau peak of the maximum amplitude to the the r.m.s of the 100th sample over an ensemble of 1000 pulses.

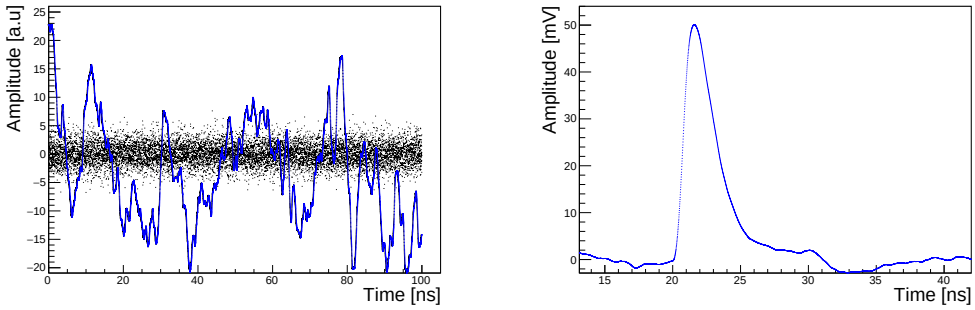

Figure 3: (Left) Comparison of gaussian white noise before and after the FEE. (Right) Example pulse at the output of the FEE block with a SNR of 30. Both figure use a shaping time (ST) of 1 ns. Legends for the shaping times are shown in the plots.

3. Timing Reconstruction and Analysis

The time reconstruction is base on a waveform analysis. We generate an ensamble of 1000 pulses sampled every 10 ps. Each pulse is interpolated using a the WhittakerShannon formula (sin(x)/x), using the interpolated pulse we assign a timestamp by finding when each pulse crosses a voltage threshold. The theshold can be a constant value (LE) or a constant fraction of the maximum amplitude of pulse (CFD), more details about the algorithms are given in Sec. 3.1. The time resolution is estimated by the width parameter of a gaussian fit to the timestamps obtain for a particular theshold. We apply a time time-walk correction based on the time-over-threshold of the pulse, we note that this correction has a large improvement on the time resolution measured using the LE algorithm while the CFD algorithm is mostly insentive to this correction. Details about this

correction are covered in Sec. 3.2. The timestamps are measured with a 20 ps binning while the time-over-thershold is measured with a 100 ps in order to simulate the effect of quantization. We scan the LE and CFD threshold such that we find the one with the lowest jitter.

3.1. Leading edge and constant fraction discriminators

The leading edge and constant fraction discriminator algorithms are ideal in the sense that they don't simulate the effect of electronics in a real implementation. The approach taken is to sample the pulses every 10 ps and subsequently interpolate them using a the WhittakerShannon formula (sin(x)/x) to more accurately find the threshold crossing. In the LE case the theshold is scanned from 3 - 60 mV, while the CFD is scanned from 5 - 90 % of the current pulse maximum amplitude. For each thershold we obtain two timestamps: when the pulse first crosses the threshold (t_0) and when it crosses the second time (t_1), now in the opposite direction. The time-over-thershold is defined as the difference of the two timestapms (ToT $= t_1 - t_0$). The first timestamp, t_0, is used to determine the time resolution at given threshold. The time resolution is defined as the width of a gaussian fit to the t_0 distribution binned with a bin-width of 20 ps. The time resolution is obtained in two cases: before and after a time-walk correction. The time-walk correction aims to correct the known drift effect on the timestamps when dealing with pulses of different amplitudes. The time walk correction is based on the measured ToT and explained in detail in Sec. 3.2. We note that the effect of the time-walk correction is large for LE and almost negligible for CFD. Fig. 4 shows a typical t_0 distribution, using the LE and CFD algorithms, for the pre-radiation LGAD after the ToT correction has been applied. The time resolution (σ_t) is measured to be 37.6 ± 2.0 and 32.9 ± 1.4 for the LE and CFS, respectively.

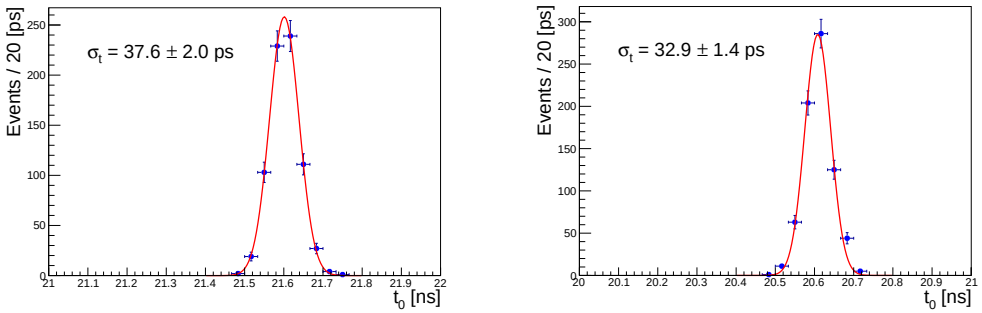

Figure 4: (Left) timestamp (t_0) distribution for a 30 mV threshold using a leading edge discriminator. (Left) timestamp (t_0) distribution for a 35% threshold using a constant fraction discriminator. Both figures include the time-walk correction based on the measured ToT. Both figures use a shaping time (ST) of 1 ns and correspond to SNR of 30.

3.2. Time-walk correction and time-over-threshold

A time-walk correction is applied in order to correct the timestamp drift when dealing with pulse of varying amplitudes. The correction is based on the measured time-over-therhold: ToT $= t_1 - t_0$. We observe, as expected, that ToT correction is large for the

LE case and negligible for CFD. Figure (left) 5 show a typical two dimensional map of t_0 and ToT for the LE algorith, wherein a clear correlation between t_0 and ToT is observed. The time-walk correction is obtain by measuring the average t_0 in each ToT bin and subsequently fitting a 2th-order polinomial (see Fig. (right) 5). The resulting analytical expresion after the fit is then used to correct the dependece of t_0 on ToT. The time-walk correction is expressed in Eq. 3, where p_2 and p_1 are the quadratic and linear coefficients of the 2th-oder polinomial fit.

$$t_0 = t_0 - (p_2 \mathrm{ToT}^2 + p_1 \mathrm{ToT}) \tag{3}$$

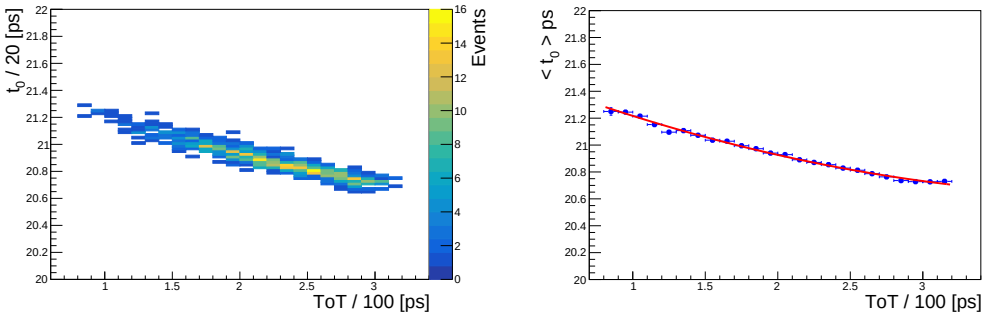

Figure 5: (Left) two dimenasional map of the timestamp (t_0) and ToT ($t_1 - t_0$). (Right) one dimensional projection of the timestamp (t_0) dependence on ToT, the red curve is the 2th-order polinomial fit that ultimately is used to correct t_0. Both figures use a shaping time (ST) of 1 ns and correspond to a SNR of 30.

4. LGAD Front-end Electronics Performance

We present a number of different studies of the LGAD sensors. such that they are above the noise levels listed for each board in Sec. **??**. All measurements other than those described in Sec. **??** and 4.3 were performed at room temperature.

4.1. Front-end electronics shaping time studies

4.2. Timing Performace as a function of signal-to-noise ratio

4.3. Timing Performace as a function of irradiation

5. Conclusion

Acknowledgment

We thank the FTBF personnel and Fermilab accelerator's team for very good beam conditions during our test beam time. We also appreciate the technical support of the Fermilab SiDet department for the rapid production of wire-bonded and packaged LGAD assemblies. We would like to thank Alan Prosser and Ryan Rivera for their critical help in setting up the DAQ and trigger chain. We thank Ned Spencer, Max Wilder, and Forest McKinney-Martinez for their technical assistance, and the CNM and HPK manufacturing team. We acknowledge the help of V. Cindro and I. Mandic with the neutron irradiations.

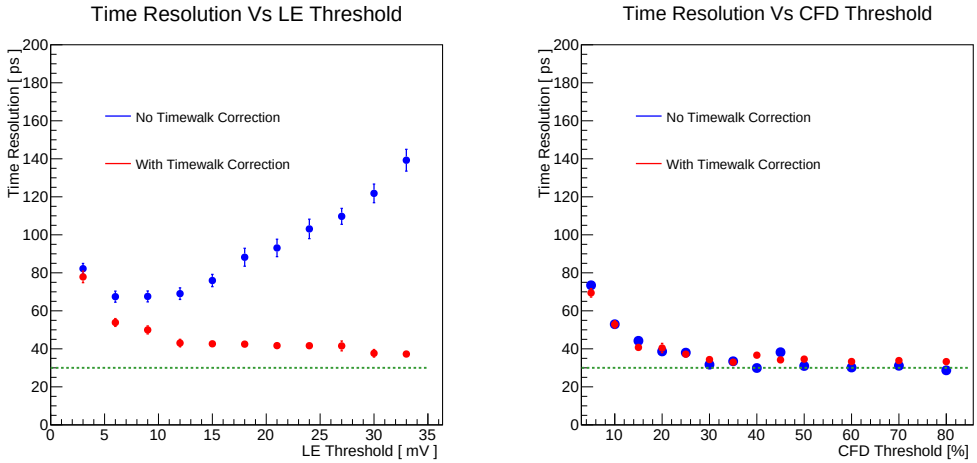

Figure 6: (Left) Comparison of gaussian white noise before and after the FEE. (Right) Example pulse at the output of the FEE block with a SNR of 30. Both figure use a shaping time (ST) of 1 ns. Legends for the shaping times are shown in the plots.

This document was prepared using the resources of the Fermi National Accelerator Laboratory (Fermilab), a U.S. Department of Energy, Office of Science, HEP User Facility. Fermilab is managed by Fermi Research Alliance, LLC (FRA), acting under Contract No. DE-AC02-07CH11359. Part of this work was performed within the framework of the CERN RD50 collaboration.

This work was supported by the Fermilab LDRD 2017.027; by the United States Department of Energy grant DE-FG02-04ER41286; by the California Institute of Technology High Energy Physics under Contract DE-SC0011925; by the European Union's Horizon 2020 Research and Innovation funding program, under Grant Agreement no. 654168 (AIDA-2020) and Grant Agreement no. 669529 (ERC UFSD669529); by the Italian Ministero degli Affari Esteri and INFN Gruppo V; and by the Spanish Ministry of Economy, Industry and Competitiveness through the Particle Physics National Program (ref. FPA2014-55295-C3-2-R and FPA2015-69260-C3-3-R) co-financed with FEDER funds.

References

[1] A. Apresyan, G. Bolla, A. Bornheim, H. Kim, S. Los, C. Pena, E. Ramberg, A. Ronzhin, M. Spiropulu, and S. Xie, "Test beam studies of silicon timing for use in calorimetry," *Nuclear Instruments and Methods in Physics Research Section A: Accelerators, Spectrometers, Detectors and Associated Equipment*, vol. 825, pp. 62 – 68, 2016.

[2] A. Apresyan, "Investigation of Fast Timing Capabilities of Silicon Sensors for the CMS High Granularity Calorimeter at HL-LHC," in *Proceedings, 2016 IEEE Nuclear Science Symposium and Medical Imaging Conference (NSS/MIC 2016)*, Oct 2016. `http://2016.nss-mic.org/index.php`.

[3] N. Akchurin, V. Ciriolo, E. Currs, J. Damgov, M. Fernndez, C. Gallrapp, L. Gray, A. Junkes, M. Mannelli, K. M. Kwok, P. Meridiani, M. Moll, S. Nourbakhsh, S. Pigazzini, C. Scharf, P. Silva, G. Steinbrueck, T. T. de Fatis, and I. Vila, "On the timing performance of thin planar silicon sensors," *Nuclear Instruments and Methods in Physics Research Section A: Accelerators, Spectrometers, Detectors and Associated Equipment*, vol. 859, pp. 31 – 36, 2017.

[4] A. Apresyan, S. Xie, C. Pena, *et al.*, "Studies of Uniformity of 50 μm Low-Gain Avalanche Detectors at the Fermilab Test Beam," *Nucl. Instrum. Meth.*, vol. A895, pp. 158–172, 2018.

[5] N. Cartiglia *et al.*, "Beam test results of a 16 ps timing system based on ultra-fast silicon detectors," *Nucl. Instrum. Meth. A*, vol. 850, pp. 83 – 88, 2017.

[6] G. Pellegrini, P. Fernández-Martinez, M. Baselga, C. Fleta, D. Flores, V. Greco, S. Hidalgo, I. Mandić, G. Kramberger, D. Quirion, and M. Ullan, "Technology developments and first measurements of Low Gain Avalanche Detectors (LGAD) for high energy physics applications," *Nuclear Instruments and Methods in Physics Research Section A: Accelerators, Spectrometers, Detectors and Associated Equipment*, vol. 765, pp. 12 – 16, 2014. HSTD-9 2013 - Proceedings of the 9th International.